JOURNAL OF SOLID STATE CHEMISTRY 120, 32–37 (1995)

Preparation of a New Phase Having a Cation-Ordered C-Type Rare-Earth Oxide Related Structure in the Systems Bi_2O_3–Ln_2O_3 (Ln = Sm, Eu, Gd, Tb, and Dy)

Akiteru Watanabe

National Institute for Research in Inorganic Materials, 1-1 Namiki, Tsukuba, Ibaraki, 305 Japan

Received February 7, 1995; accepted June 8, 1995

A new phase $Bi_{1-x}Ln_xO_{1.5}$ has been found in the systems Bi_2O_3–Ln_2O_3 (Ln = Sm, Eu, Gd, Tb, and Dy with x = 0.38, 0.375, 0.275–0.40, 0.275–0.35, and 0.30–0.35, respectively). The repetitive long-term solid-state reaction at about 800°C has produced the present phase; this phase crystallizes in the cubic system $I2_13$ with $a \approx 11$ Å and $Z = 32$, has a structure closely related to the C-type rare-earth oxide one, and is the low-temperature stable phase. Upon heating, the present phase transforms smoothly into the δ-Bi_2O_3-type high-temperature stable phase around 900°C. Upon cooling, however, a rate of transition of the opposite direction is extraordinarily sluggish. This sluggishness is discussed on the basis of the ordering of cations, Bi^{3+} and Ln^{3+}, in a proposed structure. © 1995 Academic Press, Inc.

INTRODUCTION

An adding of Ln_2O_3 (Ln = lanthanoid including Y) to Bi_2O_3 has been intensively carried out (1–12) for the purpose of stabilizing δ-Bi_2O_3 which is the high-temperature modification stable between 730 and 825°C (13,14) having the oxygen-deficient fluorite-type structure with face-centered cubic (fcc) lattice (15), because excellent oxide-ion conductivity was found in this pure δ phase (2,16). However, phase-equilibrium studies in the systems Bi_2O_3–Ln_2O_3 (Ln = La–Er and Y) (17–20) revealed the existence of the low-temperature stable phase which forms a solid solution around 22.5 mole% Ln_2O_3 having a hexagonal layered structure with the space group $R\bar{3}m$, $a \approx 4$ Å, $c \approx 24$ Å, $Z = 9$ ($Bi_{1-x}Ln_xO_{1.5}$). In other words, the stabilized δ phases reported to date are metastable at lower temperatures over the compositional range below about 30 mole% Ln_2O_3 concerning these systems. Namely, the doped δ phase can be easily quenched to room temperature. On one hand, little is known about the phase equilibrium above 30 mole% Ln_2O_3 of these systems. The phases identified so far were $Bi_8La_{10}O_{27}$ (21) and a LaOF-type solid solution above about 50 mole% Ln_2O_3 for Ln = Pr, Nd, and Sm (6, 19). Thus, the aim of the present paper is to describe the novel low-temperature stable phase found recently in the systems of Bi_2O_3 with Sm_2O_3, Eu_2O_3, Gd_2O_3, Tb_2O_3, and Dy_2O_3; this phase appears around 35 mole% Ln_2O_3 and has a structure very closely related to that of the C-type rare-earth oxide.

EXPERIMENTAL PROCEDURE AND RESULTS

Polycrystalline samples of $Bi_{1-x}Ln_xO_{1.5}$ (x = 0.2–0.5) were prepared by solid-state reaction of Bi_2O_3 (99.9%, Iwaki Chemicals Ltd.) and a lanthanoid oxide (99.9%, Shin-Etsu Chemical Co., Ltd.) of which the chemical formula is Ln_2O_3 (Ln = Sm, Eu, Gd, and Dy) or Tb_4O_7. All the lanthanoid oxides were prefired for dehydration at 600–700°C in air before use. The desired proportions were accurately weighed and thoroughly mixed with ethanol in an agate mortar. After being dried naturally, the mixture was transferred into a covered platinum crucible and heated at about 800°C for 150 hr or more. The product was then quenched by an airstream to room temperature. The same heat treatment was repeated several times after intermediate grindings to complete the reaction.

All samples were analyzed by X-ray powder diffraction (XRPD) using Cu$K\alpha$ radiation. Figure 1 shows a series of XRPD patterns for $Bi_{0.675}Gd_{0.325}O_{1.5}$ typical of a sluggish solid-state reaction; each pattern was taken just after the heat treatment under the conditions inserted. The first heat treatment (Fig. 1a) produced a mixture of the Gd_2O_3-doped δ phase and another phase with the hexagonal layered structure (17–20). The second heating (Fig. 1b) generated the new phase as a major product, while the above-mentioned two phases tend to disappear explicitly. The third heat treatment (Fig. 1c) completely produced the new phase which crystallizes in the cubic system with a = 11.05 Å. Likewise, Fig. 2 represents the change of the X-ray diffractogram of $Bi_{0.675}Dy_{0.325}O_{1.5}$ with heat treatment (22). In contrast to Fig. 1a, the first heating brought about a pure, Dy_2O_3-doped δ phase. Nevertheless, the final product

0022-4596/95 $12.00

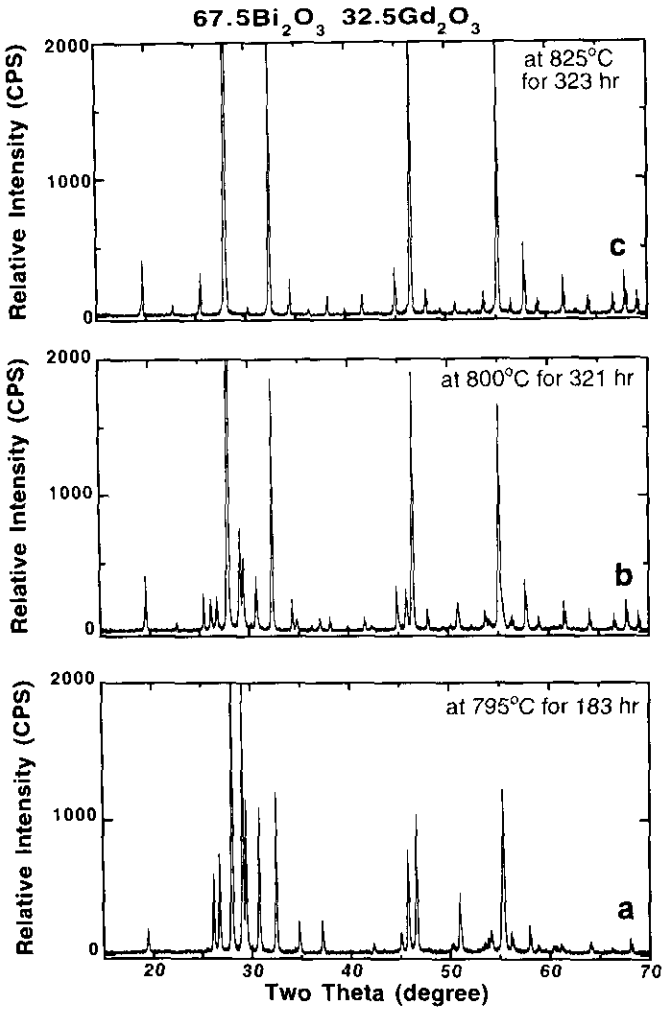

FIG. 1. The room-temperature XRPD patterns of $Bi_{0.675}Gd_{0.325}O_{1.5}$ using Cu$K\alpha$ radiation after the heat treatment under the conditions of temperature(°C)/time(hr) indicated.

(Fig. 2d) is isomorphous with that shown in Fig. 1c. The new cubic phase was identified in the following composition of each system investigated: 38 mole% Sm_2O_3, 37.5 mole% Eu_2O_3, 27.5–40 mole% Gd_2O_3, 27.5–35 mole% Tb_2O_3, and 30–35 mole% Dy_2O_3. Since all systems did not easily attain equilibrium because of the extremely sluggish solid-state reaction, the compositions of the phase boundaries are approximate values, though they are not far from the correct ones.

Since a several-times longer heat treatment might induce the compositional change by ignition loss, the composition of the new cubic phase was checked by chemical analysis using the chelatometric titration method with EDTA and xylenol orange indicator. The chosen samples are two extreme cases of the nominal compositions $Bi_{0.625}Eu_{0.375}O_{1.5}$ and $Bi_{0.62}Sm_{0.38}O_{1.5}$. Namely, in order to bring the starting powder mixture to the pure cubic phase, the former sample underwent a 10-times heat treatment, and the latter a 13-times treatment. In both samples, the conditions of each heat treatment were at about 800°C over 200 hr. The analytical results were as follows: 62.58 ± 0.02 mole% Bi_2O_3 and 37.42 ± 0.01 mole% Eu_2O_3 for $Bi_{0.625}Eu_{0.375}O_{1.5}$ and 62.04 ± 0.01 mole% Bi_2O_3 and 37.95 ± 0.01 mole% Sm_2O_3 for $Bi_{0.62}Sm_{0.38}O_{1.5}$. The compositional changes are negligibly small. That is, the actual compositions are virtually equal to the nominal ones despite of the continual long heating.

Figure 3 exhibits the indexed XRPD pattern of the new cubic phase of $Bi_{0.65}Gd_{0.35}O_{1.5}$. The observable reflections are hkl, $h + k + l = 2n$; this condition indicates a body-centered cubic (BCC) lattice and leads to the possible space groups $Im3m$, $I432$, $I\bar{4}3m$, $Im3$, I23, and $I2_13$. In a later section it is shown that $I2_13$ is reasonably selected

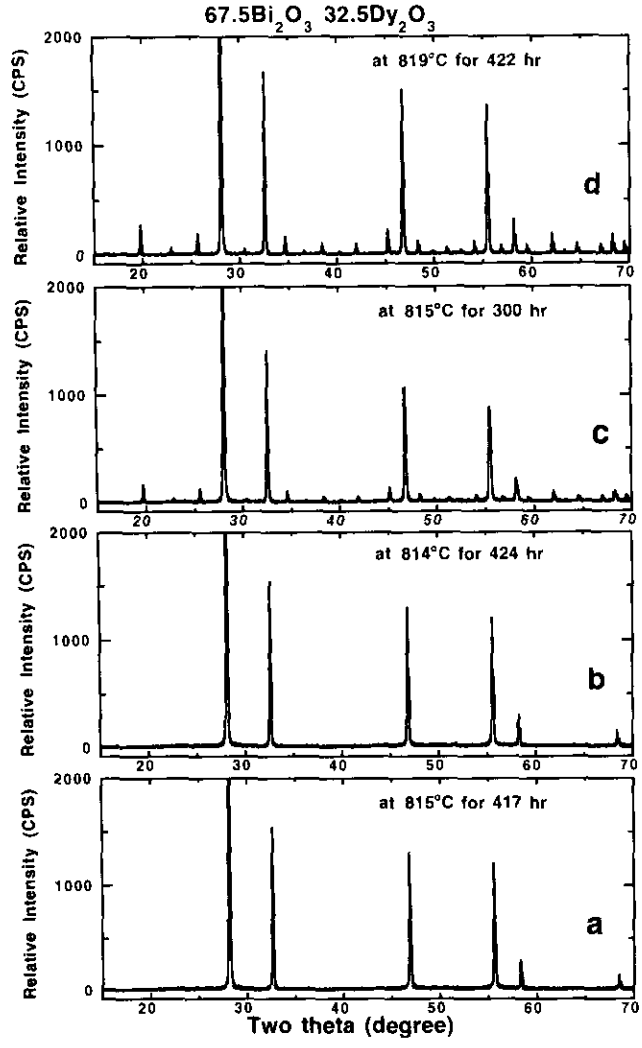

FIG. 2. The room-temperature XRPD patterns of $Bi_{0.675}Dy_{0.325}O_{1.5}$ after the heat treatment under the conditions of temperature(°C)/time(hr) indicated (22). Radiation Cu$K\alpha$.

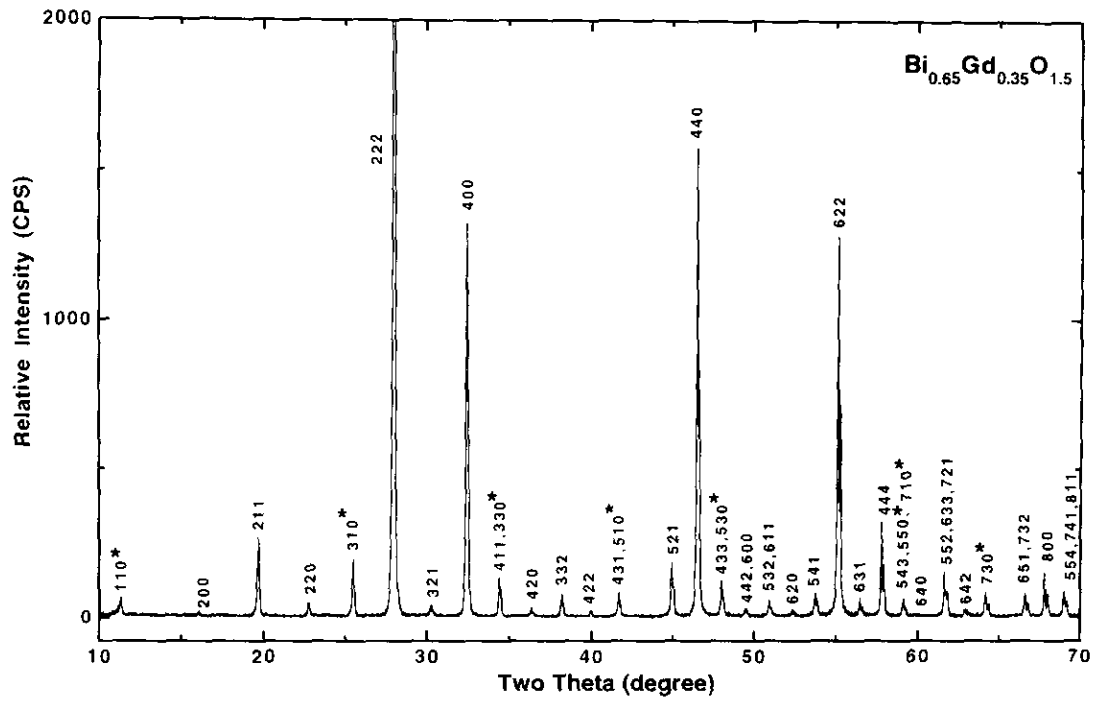

FIG. 3. The XRPD pattern of a new body-centered cubic phase with $Bi_{0.65}Gd_{0.35}O_{1.5}$. The asterisked indices are of the type $hk0$ with $h = 2n + 1$ and $k = 2n + 1$.

from the structural point of view. Hereafter, we designate the present new cubic phase the BCC phase for convenience.

The precise lattice constant was determined by applying the least-squares treatment to 36 independent reflections selected in the $2\theta = 70°$–$120°$ region with Cu$K\alpha$ radiation and a diffracted-beam monochromator. The measured 2θ values were corrected using an external standard of Si powder. The results are tabulated in Table 1. At the same time, for structural studies, integrated intensities were measured from X-ray diffraction patterns with the background corrections; the patterns were recorded between 2θ values 10° and 90° with the continuous scanning measurement at a scanning rate of 0.4° min^{-1}. Table 2 gives the observed and calculated d values and measured integrated intensities for $Bi_{0.65}Gd_{0.35}O_{1.5}$.

TABLE 1
Lattice Parameters of $Bi_{1-x}Ln_xO_{1.5}$

Ln	*x*	*a* (Å)	*V* (Å)
Sm	0.380	11.1017(1)	1368.29(4)
Eu	0.375	11.0722(0)	1357.38(2)
Gd	0.275	11.0531(1)	1350.37(4)
Gd	0.300	11.0530(0)	1350.35(3)
Gd	0.325	11.0523(0)	1350.08(3)
Gd	0.350	11.0510(0)	1349.62(6)
Gd	0.375	11.0506(0)	1349.45(2)
Gd	0.400	11.0461(0)	1347.82(2)
Tb	0.275	11.0198(1)	1338.21(6)
Tb	0.300	11.0207(1)	1338.53(4)
Tb	0.325	11.0192(0)	1338.00(3)
Tb	0.350	11.0196(0)	1338.14(3)
Dy	0.300	10.9873(1)	1326.42(4)
Dy	0.325	10.9872(0)	1326.35(3)
Dy	0.350	10.9869(1)	1326.25(4)

The density measurement was done by gas pycnometer (Micromeritics Accupyc 1330). The results were 8.442 ± 0.006 g cm^{-3} for $Bi_{0.65}Gd_{0.35}O_{1.5}$ and 8.578 ± 0.003 g cm^{-3} for $Bi_{0.675}Tb_{0.325}O_{1.5}$.

The thermal behavior was checked by a conventional differential thermal analysis (DTA) apparatus. About 100 mg of pulverized sample underwent heating–cooling cycles at a rate of 10°C min^{-1} and a maximum temperature of 1100°C. The reference material was α-Al_2O_3. Figure 4 shows a typical thermogram for the present BCC phase of $Bi_{0.675}Dy_{0.325}O_{1.5}$: an extremely widespread endothermic peak was detected around 900°C only in the first heating direction. The same thermal behavior was observed for each of the other systems. An onset temperature of the broad endothermic peak was adopted as an approximate transition temperature. That of the representative composition in each system was as follows: ca. 890°C for 38 mole% Sm_2O_3, ca. 900°C for 37.5 mole% Eu_2O_3, ca. 890°C for 35 mole% Gd_2O_3, ca. 890°C for 35 mole% Tb_2O_3, and ca. 900°C for 35 mole% Dy_2O_3. No thermal effect was observed on the traces through the subsequent cooling pro-

TABLE 2
X-Ray Powder Diffraction Data for $Bi_{0.65}Gd_{0.35}O_{1.5}$

h k l	d_{calc} (Å)	d_{obs} (Å)	I_{obs}	I_{calc}
1 1 0	7.814	7.800	2.6	0.1
2 0 0	5.526	5.521	0.8	0.9
2 1 1	4.516	4.511	7.4	6.0
2 2 0	3.907	3.905	1.8	1.7
3 1 0	3.495	3.493	5.5	2.3
2 2 2	3.1902	3.1892	*100.0*	*100.0*
3 2 1	2.9535	2.9537	1.4	3.2
4 0 0	2.7628	2.7620	35.0	38.3
3 3 0	2.6048	2.6046	4.3	4.0
4 2 0	2.4711	2.4705	1.1	1.3
3 3 2	2.3561	2.3554	2.3	2.5
4 2 2	2.2558	2.2547	0.8	0.4
5 1 0	2.1673	2.1667	2.6	4.8
5 2 1	2.0176	2.0172	6.3	1.7
4 4 0	1.9536	1.9533	36.4	35.8
5 3 0	1.8952	1.8952	3.6	1.8
6 0 0	1.8418	1.8416	1.1	0.7
6 1 1	1.7927	1.7922	2.2	3.2
6 2 0	1.7473	1.7477	1.0	0.9
5 4 1	1.7052	1.7053	3.0	3.6
6 2 2	1.6660	1.6658	34.2	31.9
6 3 1	1.6294	1.6296	2.4	4.1
4 4 4	1.5951	1.5952	9.6	7.8
5 5 0	1.5629	1.5628	2.3	2.5
7 2 1	1.5039	1.5048	5.1	3.3
6 4 2	1.4768	1.4769	0.9	1.1
7 3 0	1.4511	1.4509	2.9	0.5
6 5 1	1.4035	1.4034	2.7	2.1
8 0 0	1.3814	1.3813	5.2	3.6
7 4 1	1.3603	1.3603	3.1	3.4
8 2 0	1.3401	1.3402	0.7	1.0
6 5 3	1.3209	1.3208	0.9	1.5
6 6 0	1.3024	1.3023	1.2	0.3
7 5 0	1.2847	1.2847	2.4	2.3
6 6 2	1.2676	1.2677	12.0	8.7
8 4 0	1.2356	1.2354	10.0	7.2
9 1 0	1.2204	1.2203	1.2	0.5
8 4 2	1.2058	1.2058	1.4	1.0
7 6 1	1.1917	1.1916	3.6	2.4
9 3 0	1.1649	1.1649	2.3	2.7
9 3 2	1.1398	1.1398	2.2	2.0
8 4 4	1.1279	1.1279	7.6	4.9
7 7 0	1.1163	1.1164	2.8	2.5
7 7 2	1.0942	1.0943	1.3	0.7

cess and the second heating–cooling run. An XRPD pattern of each sample after DTA measurement exhibited the FCC lattice, viz., the doped δ phase. This result indicates that the low-temperature stable BCC phase transforms irreversibly into the high-temperature stable, doped δ phase. As is evident from Figs. 1 and 2, however, this irreversibility is only apparent. Namely, a rate of transition from the δ to the BCC phase is extraordinarily sluggish in contrast to that of the opposite direction from the BCC to the δ phase.

In general, however, DTA does not distinguish between thermodynamically stable and metastable phases. Thus, the stability of the present BCC phase was checked further in the following ways in the system Bi_2O_3–Gd_2O_3. A doped δ phase specimen with composition $Bi_{0.65}Gd_{0.35}O_{1.5}$ was easily prepared by a solid-state reaction at 950°C for 60 hr; next, the obtained δ phase was annealed at 795°C for 105 hr. As a result, it turned out that the doped δ phase transformed perfectly into the BCC phase. An alternate method of confirming the stability of the BCC phase was pursued on the basis of the following solid-state reaction:

$$5Bi_{0.75}Gd_{0.25}O_{1.5} + 2Bi_{0.4}Gd_{0.6}O_{1.5} \rightarrow 7Bi_{0.65}Gd_{0.35}O_{1.5}.$$

In the reactants, $Bi_{0.75}Gd_{0.25}O_{1.5}$ and $Bi_{0.4}Gd_{0.6}O_{1.5}$ are pure phases with the hexagonal layered structure (17–20) and the LaOF-type structure (23), respectively. Both phases were prepared in advance by solid-state reaction. Their stoichiometric mixture was heated first at 802°C for 113 hr; the product was a three-phase mixture of the doped δ phase and the two starting substances. A second heating at 825°C for 323 hr produced only the pure BCC phase according to the above reaction. Now that it is possible to generate the present BCC phase in different ways, it is clearly proven that the BCC phase is the truly low-temperature stable phase. At the same time, it is noted that the doped δ phase was generated even at lower temperatures than the polymorphic transition temperature around 900°C (Figs. 1 and 2). We discuss this problem afterward.

DISCUSSION

The XRPD pattern shown in Fig. 3 agrees well with that of the pure C-type rare-earth oxides, such as Sm_2O_3 and Eu_2O_3 (24), if we remove asterisked $hk0$ reflections from

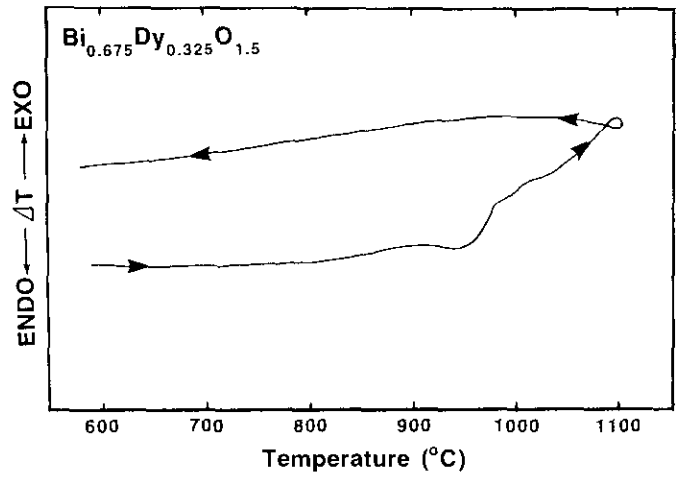

FIG. 4. DTA curve in the heating and cooling cycle for $Bi_{0.675}Dy_{0.325}O_{1.5}$.

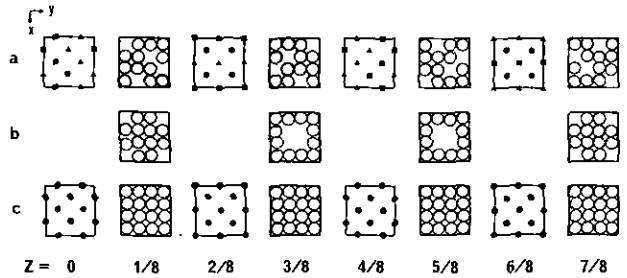

FIG. 5. Crystal structures depicted in a series of cross sections. (a) Idealized structure of the present new bcc phase based on $I2_13$: solid circles denote *Ln* atoms, solid squares and triangles are atoms occupied statistically by Bi and *Ln*, and open circles are O atoms. (b) Arrangement of O atoms based on the space groups *Im*3*m*, *I*432, *I*43*m*, *Im*3, and *I*23. (c) Eight unit cells of δ-Bi_2O_3-type structure (fluorite-type); solid circles are Bi atoms and open circles are O atoms of which only 75% are statistically occupied.

Fig. 3, in which h and k are all odd, especially singlet ones such as 110 and 310; a systematic absence occurs for such $hk0$ reflections in the C-type rare-earth oxide structure with the space group *Ia*3. This remarkable resemblance denotes that the structure of the present BCC phase is closely related to that of the C-type rare-earth oxide. Accordingly, an outline of the crystal structure for the BCC phase was checked in the following on referring to the structure of the C-type rare-earth oxide (25).

From the density value and lattice constant, it is clear that the unit cell of the BCC phase contains 32 formula weights, $Z = 32(Bi_{1-x}Ln_xO_{1.5})$, in the same manner as the C-type rare-earth oxide structure. Consequently, there exist 48 oxygen atoms in the unit cell. In the light of the spatial arrangement of these 48 oxygen atoms, the six candidates (*Im*3*m*, *I*432, $I\bar{4}3m$, *Im*3, *I*23, and $I2_13$) for the correct space group were examined. The general positions were assigned to them, viz., 48*j* for *I*432, two sets of 24*c* for $I2_13$, etc., except for *Im*3*m* where 48*k* special positions were employed. As a result, only the space group $I2_13$ gave a reasonable atomic arrangement shown in Fig. 5a. These positions are in fairly good agreement with those of the C-type rare-earth oxide structure. In contrast, the other space groups led to the irrational oxygen positions which are not distributed uniformly in the unit cell as shown in Fig. 5b. Therefore, we examined the positions of cations on the basis of the space group $I2_13$. As noted above, the strong resemblance between the XRPD pattern of the BCC phase and that of the C-type rare-earth oxide suggests that the relative atomic positions may be similar to those of the C-type rare-earth oxide structure. In addition, the appearance of the extra reflections ($hk0$ with $h = 2n + 1$ and $k = 2n + 1$) implies the existence of atomic ordering in cation sublattices. We may infer from these matters an outline of the BCC structure. First, we shall assign the eight *Ln* atoms to the special positions 8*a*. The other 24 cations, $(32x - 8)Ln$ and $32(1 - x)$Bi atoms, can statistically occupy just two sets of the special positions 12*b*. All the O atoms are split into two sets and can occupy the positions 24*c*. The positional parameters thus estimated are listed in Table 3. Also a mode of the cation ordering is depicted in Fig. 5a. The calculated intensities juxtaposed in Table 2 are based on these atomic coordinates with an overall temperaure parameter $B = 1.4$ in $\exp[-2B(\sin\theta/\lambda)^2]$. An agreement index, $R_I = \Sigma_{hkl}|I_{obs} - I_{cal}|/\Sigma_{hkl}I_{obs}$, for the 44 reflections listed in Table 2 was 15.5%. To determine the correct structure, a single crystal X-ray diffraction analysis is needed. However, it is very difficult to obtain the single crystal of the BCC phase, because the primary phase from the melt is always the δ phase. Thus, the structure determination by Rietveld method is now under investigation.

As mentioned in the Introduction, the δ phase exhibits a good oxide-ion conduction because of the oxygen-deficient fluorite-type structure in which the oxygen sublattice contains 25% defects. On the other hand, since both cation sites and oxygen sites of the proposed BCC structure are fully occupied, the oxide-ion conductivity of the BCC phase might be lower than that of the Ln_2O_3-doped δ phase. In fact, the electrical conductivity of the BCC phase with $Bi_{0.65}Gd_{0.35}O_{1.5}$ was more than 100 times lower than that of the corresponding doped δ phase (22). This result supports the proposed structural model of the BCC phase.

The structure of the BCC phase is also closely connected with that of the doped δ phase as shown in Fig. 5. Thus, there is little difference in the positions of cations between the ordered lattice of the BCC phase and the completely disordered lattice of the doped δ phase. As for the distribution of cations, however, there is a large difference between the two phases. Accordingly we can imagine that the formation of the ordered lattice in the BCC phase may be still more difficult than that of the disordered lattice in the doped δ phase, taking a similarity of ionic radii between the same valent Bi^{3+} and Ln^{3+} into consideration. That is, it is the cation-ordering process that may be the transition-rate-determining step or the time-consuming one. This cat-

TABLE 3
Proposed Atomic Coordinates for the New $Bi_{1-x}Ln_xO_{1.5}$ Phase in the Space Group $I2_13$[a]

Atom		*x*	*y*	*z*
Ln	8*a*	0.270	0.270	0.270
M(1)[b]	12*b*	−0.021	0	0.25
M(2)[b]	12*b*	0.479	0	0.25
O(1)	24*c*	0.370	0.087	0.350
O(2)	24*c*	0.120	0.338	0.100

[a] $Z = 32$.
[b] $M = [(32x - 8)/24]Ln + [32(1 - x)/24]$Bi.

ion order–disorder arrangement difference explains both the sluggish transition rate from the doped δ phase to the BCC phase and the apparent irreversibility of thermal effect detected on the DTA traces.

As is evident from Figs. 1 and 2, the doped δ phase was easily produced at temperatures much lower than the transition temperature. These results indicate that the present systems obey the "Ostwald step rule"—when a compound with some modifications crystallizes, first a thermodynamically unstable modification may be generated under the given conditions, and then it transforms to the more stable modification. Probably the above-mentioned cation ordering difficulty seems to give rise to this rule in the present systems. Thus, since the doped δ phase is first formed and cooled metastably to room temperature, it might well be erroneously identified as the stable phase. Furthermore, since the high-temperature stable, doped δ phase stands against the transformation into the low-temperature stable BCC phase despite long-term annealing at lower temperatures than the transition temperature, the BCC phase has never been found to date.

ACKNOWLEDGMENT

The author thanks Mr. S. Takenouchi for checking the sample composition by chemical analysis.

REFERENCES

1. T. Takahashi, H. Iwahara, and Y. Nagai, *J. Appl. Electrochem.* **2,** 97 (1972).
2. T. Takahashi, H. Iwahara, and T. Arao, *J. Appl. Electrochem.* **5,** 187 (1975).
3. T. Takahashi, T. Esaka, and H. Iwahara, *J. Appl. Electrochem.* **5,** 197 (1975).
4. M. J. Verkerk, K. Keizer, and A. J. Burggraaf, *J. Appl. Electrochem.* **10,** 81 (1980).
5. H. T. Cahen, T. G. M. van den Belt, J. H. W. de Wit, and G. H. J. Broers, *Solid State Ionics* **1,** 411 (1980).
6. H. Iwahara, T. Esaka, T. Sato, and T. Takahashi, *J. Solid State Chem.* **39,** 173 (1981).
7. M. J. Verkerk and A. J. Burggraaf, *J. Electrochem. Soc.* **128,** 75 (1981).
8. H. Kruidhof, K. Seshan, B. C. Lippens Jr., P. J. Gellings, and A. J. Burggraaf, *Mater. Res. Bull.* **22,** 1635 (1987).
9. H. Kruidhof, K. Seshan, G. M. H. van de Velde, K. J. de Vries, and A. J. Burggraaf, *Mater. Res. Bull.* **23,** 371 (1988).
10. H. Kruidhof, K. J. de Vries, and A. J. Burggraaf, *Solid State Ionics* **37,** 213 (1990).
11. H. Kruidhof, H. J. M. Bouwmeester, K. J. de Vries, P. J. Gellings, and A. J. Burggraaf, *Solid State Ionics* **50,** 181 (1992).
12. N. H. Sammes and G. J. Gainesford, *Solid State Ionics* **62,** 179 (1993).
13. E. M. Levin and R. S. Roth, *J. Res. Nat. Bur. Stand. U.S.A. Sect. A* **68,** 189 (1964).
14. H. A. Harwig and A. G. Gerards, *Thermochim. Acta* **28,** 121 (1979).
15. H. A. Harwig, *Z. Anorg. Allg. Chem.* **444,** 151 (1978).
16. M. G. Hapase and V. B. Tare, *Indian J. Pure Appl. Phys.* **5,** 401 (1967).
17. A. Watanabe and T. Kikuchi, *Solid State Ionics* **21,** 287 (1986).
18. A. Watanabe, *Solid State Ionics* **34,** 35 (1989).
19. P. Conflant, C. Follet-Houttemane, and M. Drache, *J. Mater. Chem.* **1,** 649 (1991).
20. A. Watanabe, M. Drache, J.P. Wignacourt, P. Conflant, and J. C. Boivin, *Solid State Ionics* **67,** 25 (1993).
21. C. Michel, V. Caignaert, and B. Raveau, *J. Solid State Chem.* **90,** 296 (1991).
22. A. Watanabe, *Solid State Ionics* **79,** 84 (1995).
23. A. Watanabe, unpublished data.
24. JCPDS cards: 12-797, 15-813, 22-612, 23-1418, 34-392.
25. A. F. Wells, "Structural Inorganic Chemistry," 4th ed., p. 450. Clarendon, Oxford, 1975.